

Curvature-induced optical phonon frequency shift in metallic carbon nanotubes

Ken-ichi Sasaki,¹ Riichiro Saito,¹ Gene Dresselhaus,² Mildred S. Dresselhaus,^{3,4} Hootan Farhat,⁵ and Jing Kong⁴

¹*Department of Physics, Tohoku University and CREST-JST, Sendai 980-8578, Japan*

²*Francis Bitter Magnet Laboratory, Massachusetts Institute of Technology, Cambridge, Massachusetts 02139-4307, USA*

³*Department of Physics, Massachusetts Institute of Technology, Cambridge, Massachusetts 02139-4307, USA*

⁴*Department of Electrical Engineering and Computer Science, Massachusetts Institute of Technology,*

Cambridge, Massachusetts 02139-4307, USA

⁵*Department of Materials Science and Engineering, Massachusetts Institute of Technology, Cambridge, Massachusetts 02139-4307, USA*

(Received 21 March 2008; revised manuscript received 25 April 2008; published 27 June 2008)

The quantum corrections to the frequencies of the Γ point longitudinal-optical (LO)- and transverse-optical (TO)-phonon modes in carbon nanotubes are investigated theoretically. The frequency shift and broadening of the TO-phonon mode strongly depend on the curvature effect due to a special electron-phonon coupling in carbon nanotubes, which is shown by the Fermi energy dependence of the frequency shift for different nanotube chiralities. It is also shown that the TO mode near the Γ point decouples from electrons due to local gauge symmetry and that a phonon mixing between LO and TO modes is absent due to time-reversal symmetry. Some comparisons between theory and experiment are presented.

DOI: [10.1103/PhysRevB.77.245441](https://doi.org/10.1103/PhysRevB.77.245441)

PACS number(s): 61.46.-w, 63.22.-m

I. INTRODUCTION

In the Raman spectra of a single-wall carbon nanotube (SWNT), the two in-plane optical-phonon modes, that is, the longitudinal-optical (LO)- and transverse-optical (TO)-phonon modes at the Γ point in the two-dimensional Brillouin zone (2D BZ), which are degenerate in graphite and graphene, split into two peaks, G^+ and G^- peaks, respectively.¹⁻³ The splitting of the two peaks for SWNTs is inversely proportional to the square of the diameter d_t of SWNTs due to the curvature effect, in which G^+ does not change with changing d_t , but the G^- frequency decreases with decreasing d_t .^{4,5} In particular, for metallic SWNTs, the G^- peaks appear at a lower frequency than the G^+ peaks for semiconducting SWNTs with a similar diameter.⁶ The spectra of G^- for metallic SWNTs show a much larger spectral width than that of semiconducting SWNTs. Further, the spectral G^- feature shows an asymmetric line shape as a function of frequency, which is known as the Breit-Wigner-Fano (BWF) line shape.⁷ The origin of the BWF line shape is considered to be due to the interaction of discrete phonon states with continuous free-electron states.

It has been widely accepted that the frequency shift of the G band is produced by the electron-phonon (el-ph) interaction.⁸⁻¹³ An optical phonon changes into an electron-hole pair as an intermediate state by the el-ph interaction. This process gives the phonon a self-energy. The phonon self-energy is sensitive to the Fermi energy, E_F . In the case of graphite intercalation compounds in which the charge transfer of an electron from a dopant to the graphite layer can be controlled by the doping atom and its concentration, Eklund *et al.*¹⁴ observed a shift of the G -band frequency with an increase in the spectral width. The frequency shifted spectra show that not only the LO mode but also the TO mode are shifted in the same fashion by a dopant. For a graphene monolayer, Lazzeri *et al.*⁹ calculated the E_F dependence of the shift of the G -band frequency. The LO mode softening in metallic SWNTs was shown by Dubay *et al.*^{15,16} on the basis

of density-functional theory. Recently Nguyen *et al.*¹⁷ and Farhat *et al.*¹⁸ observed the phonon-softening effect of SWNTs as a function of E_F by field effect doping and electrochemical doping, respectively, and their results clearly show that the LO-phonon modes become soft as a function of E_F . Ando¹⁹ discussed the phonon softening of metallic SWNTs as a function of the E_F position, in which the phonon softening occurs for the LO-phonon mode and for a special range of E_F , that is, for $|E_F| < \hbar\omega_{LO}/2$.

In this paper, we show that the Γ point TO-phonon mode becomes hard when $|E_F| \lesssim \hbar\omega_{TO}/2$ and has a considerable broadening for metallic zigzag nanotubes. The occurrence of the phonon hardening for the TO mode is due to the curvature effect, a special character of the el-ph coupling, and a basic consequence of second-order perturbation theory. We show using a gauge symmetry argument that the electrons completely decouple from the TO mode near the Γ point. Besides, we show that for a chiral nanotube, both the LO and TO modes are softened due to the fact that the direction of the TO-phonon vibration is not parallel to the nanotube circumferential direction.²⁰ Another interest of ours is the mixing of LO and TO phonons to form degenerate phonon frequencies. When the LO-phonon mode becomes soft, a crossing of the LO mode with the TO mode occurs at a certain value of E_F . For such a mode crossing, we should generally consider the el-ph coupling for degenerate phonon modes to sense the crossing or anticrossing of the two phonon frequencies as a function of E_F . We show by an analytical calculation that there is no mixing between the LO- and TO-phonon modes for any case due to time-reversal symmetry.

The organization of the paper is as follows. In Sec. II we show our method of calculation and present the results for armchair and metallic zigzag SWNTs. In Sec. III using effective-mass theory, we show how the el-ph interaction depends on the chiral angles of SWNTs, and in Sec. IV a discussion based on gauge symmetry and time-reversal symmetry for the el-ph coupling is given. In Sec. V, a comparison with the experiments and a summary are given.

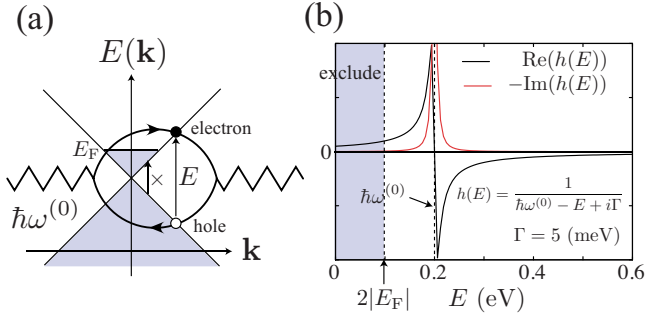


FIG. 1. (Color online) (a) An intermediate electron-hole pair state that contributes to the energy shift of the optical phonon modes is depicted. A phonon mode is denoted by a zigzag line and an electron-hole pair is represented by a loop. The low-energy electron-hole pair satisfying $0 \leq E \leq 2|E_F|$ is forbidden at zero temperature by the Pauli principle. (b) The energy correction to the phonon energy by an intermediate electron-hole pair state, especially the sign of the correction, depends on the energy of the intermediate state as $h(E)$. (See text.)

II. PHONON-FREQUENCY SHIFT

The frequency shift of the Γ -point LO- and TO-phonon modes for metallic SWNTs is calculated by second-order perturbation theory. The phonon energy, including the el-ph interaction, becomes $\hbar\omega_\lambda = \hbar\omega_\lambda^{(0)} + \hbar\omega_\lambda^{(2)}$ ($\lambda = \text{LO, TO}$), where $\omega_\lambda^{(0)}$ is the original phonon frequency without the el-ph interaction and the correction term $\hbar\omega_\lambda^{(2)}$ is given by

$$\hbar\omega_\lambda^{(2)} = 2 \sum_{\mathbf{k}} \frac{|\langle \text{eh}(\mathbf{k}) | \mathcal{H}_{\text{int}} | \omega_\lambda \rangle|^2}{\hbar\omega_\lambda^{(0)} - [E_e(\mathbf{k}) - E_h(\mathbf{k})] + i\Gamma_\lambda} \times \{f[E_h(\mathbf{k}) - E_F] - f[E_e(\mathbf{k}) - E_F]\}. \quad (1)$$

The factor 2 in Eq. (1) comes from spin degeneracy. $\hbar\omega_\lambda^{(2)}$ is the quantum correction to the phonon energy due to the electron-hole pair creation, as shown in Fig. 1(a). In Eq. (1), $\langle \text{eh}(\mathbf{k}) | \mathcal{H}_{\text{int}} | \omega_\lambda \rangle$ is the matrix element for creating an electron-hole pair at momentum \mathbf{k} by the el-ph interaction, \mathcal{H}_{int} , $E_e(\mathbf{k})$ [$E_h(\mathbf{k})$] is the electron (hole) energy, and Γ_λ is the decay width. In Fig. 1(a), an intermediate electron-hole pair state that has the energy of $E = E_e(\mathbf{k}) - E_h(\mathbf{k})$ is shown. We need to sum ($\sum_{\mathbf{k}}$) over all possible intermediate electron-hole pair states in Eq. (1), which can have a much larger energy than the phonon ($E \gg \hbar\omega_\lambda^{(0)}$).

Since $\langle \text{eh}(\mathbf{k}) | \mathcal{H}_{\text{int}} | \omega_\lambda \rangle$ is a smooth function of $E = E_e(\mathbf{k}) - E_h(\mathbf{k})$ in the denominator of Eq. (1), the contribution to $\hbar\omega_\lambda^{(2)}$ from an electron-hole pair depends on its energy. In Fig. 1(b), we plot the real part and imaginary part of the denominator of Eq. (1), $h(E) = 1 / (\hbar\omega_\lambda^{(0)} - E + i\Gamma)$ as a function of E in the case of $\hbar\omega_\lambda^{(0)} = 0.2$ eV and $\Gamma = 5$ meV. Here $\text{Re}[h(E)]$ has a positive (negative) value when $E < \hbar\omega_\lambda^{(0)}$ ($E > \hbar\omega_\lambda^{(0)}$) and the lower (higher) energy electron-hole pair makes a positive (negative) contribution to $\hbar\omega_\lambda^{(2)}$. Moreover, an electron-hole pair satisfying $E < 2|E_F|$ cannot contribute to the energy shift [shaded region in Figs. 1(a) and 1(b)] because of the Fermi distribution function f in Eq. (1). Thus, the quantum correction to the phonon energy by an intermediate electron-hole pair can be controlled by changing the

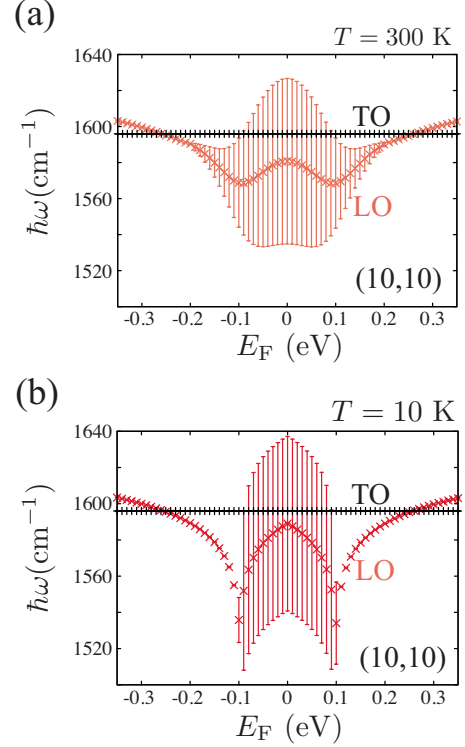


FIG. 2. (Color online) The E_F dependence of the LO (red curve) and TO (black curve) phonon energy in the case of the (10,10) armchair nanotube. (a) is taken at room temperature and (b) is at 10 K. Only the energy of the LO mode is shifted, with the TO mode frequency being independent of E_F . The decay width (Γ_λ) is plotted as an error bar.

Fermi energy, E_F . For example, when $|E_F| = \hbar\omega_\lambda^{(0)}/2$, then $\hbar\omega_\lambda^{(2)}$ takes a minimum value at zero temperature since all positive contributions to $\hbar\omega_\lambda^{(2)}$ are suppressed in Eq. (1). Since $\text{Re}[h(E)] \approx -1/E$ for $E \gg \hbar\omega_\lambda^{(0)}$, all high-energy intermediate states contribute to phonon softening if we include all the electronic states in the system.¹⁰ Here we introduce a cutoff energy at $E_c = 0.5$ eV as $\sum_{\mathbf{k}}^{E_e(\mathbf{k}) < E_c}$ in order to avoid such a large energy shift in Eq. (1). The energy shift due to the high-energy intermediate states $\sum_{\mathbf{k}}^{E_e(\mathbf{k}) > E_c}$ can be neglected by renormalizing $\hbar\omega_\lambda^{(0)}$ so as to reproduce the experimental results of Raman spectra¹⁸ since the contribution from $E_e(\mathbf{k}) > E_c$ just gives a constant energy shift to $\hbar\omega_\lambda^{(2)}$. We have checked that the present results do not depend on the selection of the cutoff energy since E_c is much larger than $\hbar\omega_\lambda^{(0)}$.

$\text{Im}[h(E)]$ is nonzero only very close to $E = \hbar\omega_\lambda^{(0)}$, which shows that the phonon can resonantly decay into an electron-hole pair with the same energy. It is noted that when $|E_F| > \hbar\omega_\lambda^{(0)}/2$, $\Gamma_\lambda \approx 0$ at zero temperature while Γ_λ may take a finite value at a finite temperature. In this paper, we calculate Γ_λ self-consistently by calculating $\Gamma_\lambda = -\text{Im}(\hbar\omega_\lambda^{(2)})$ in Eq. (1).

In Fig. 2, we show calculated results for $\hbar\omega_\lambda$ as a function of E_F for a (10,10) armchair nanotube. Here we take 1595 and 1610 cm^{-1} for $\hbar\omega_\lambda^{(0)}$ for the TO and LO modes, respectively. The energy bars denote Γ_λ values. We have used the extended tight-binding scheme to calculate $E_e(\mathbf{k})$ and $E_h(\mathbf{k})$ and the electron wave function for $\langle \text{eh}(\mathbf{k}) | \mathcal{H}_{\text{int}} | \omega_\lambda \rangle$.²¹ As for

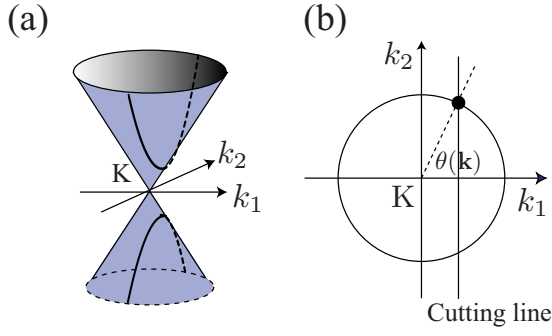


FIG. 3. (Color online) (a) Cutting line near the K point. The k_1 (k_2) axis is selected as the nanotube circumferential (axis) direction. The amplitude for an electron-hole pair creation depends strongly on the relative position of the cutting line from the K point. (b) If the cutting line crosses the K point, then the angle $\theta(k)$ ($\equiv \arctan(k_2/k_1$) takes $\pi/2$ ($-\pi/2$) values for $k_2 > 0$ ($k_2 < 0$). In this case, the LO mode strongly couples to an electron-hole pair, while the TO mode is decoupled from the electron-hole pair according to Eq. (2).

the el-ph matrix element,²² we adopted the deformation potential derived on the basis of density-functional theory by Porezag *et al.*²³ To obtain the phonon eigenvector, we used the force-constant parameters calculated by Dubay and Kresse¹⁶ for the dynamical matrix. We show the resulting $\hbar\omega_\lambda$ as a function of E_F at the room temperature ($T = 300$ K) and $T = 10$ K in Figs. 2(a) and 2(b), respectively. It is shown that the TO mode does not exhibit any energy change while the LO mode shows an energy shift and broadening. As we have mentioned above, the minimum energy is realized at $|E_F| = \hbar\omega^{(0)}/2$ (≈ 0.1 eV). There is a local maximum for the spectral peak at $|E_F| = 0$. The broadening for the LO mode occurs within $|E_F| \lesssim \hbar\omega^{(0)}/2$ for the lower temperature, while the broadening has a tail at room temperature for $|E_F| \gtrsim \hbar\omega^{(0)}/2$.

An effective-mass theory for electrons in a carbon nanotube is adopted in this paper to explain the lack of an energy shift of the TO modes for armchair nanotubes. As we will show in Sec. III, the el-ph matrix element for the electron-hole pair creation by the (A_{1g}) LO and TO modes is given by

$$\begin{aligned} \langle eh(\mathbf{k}) | \mathcal{H}_{\text{int}} | \omega_{\text{LO}} \rangle &= -igu \sin \theta(\mathbf{k}), \\ \langle eh(\mathbf{k}) | \mathcal{H}_{\text{int}} | \omega_{\text{TO}} \rangle &= -igu \cos \theta(\mathbf{k}), \end{aligned} \quad (2)$$

where u is the phonon amplitude and g is the el-ph coupling constant. Here $\theta(\mathbf{k})$ is the angle for the polar coordinate around the K (or K') point in the 2D BZ, in which the $\mathbf{k} = (k_1, k_2)$ point is taken on a cutting line for a metallic energy subband. The k_1 (k_2) axis is taken in the direction of the nanotube circumferential (axis) direction (see Fig. 3). Equation (2) shows that $\langle eh(\mathbf{k}) | \mathcal{H}_{\text{int}} | \omega_\lambda \rangle$ depends only on $\theta(\mathbf{k})$ but not on $|\mathbf{k}|$, which means that the dependence of this matrix element on E is negligible. Since the armchair nanotube is free from the curvature effect,²⁴ the cutting line for its metallic energy band lies on the k_2 axis. Thus, we have $\theta(\mathbf{k}) = \pi/2$ ($-\pi/2$) for the metallic energy subband, which has $k_1 = 0$ and $k_2 > 0$ ($k_2 < 0$). Then, Eq. (2) tells us that only the

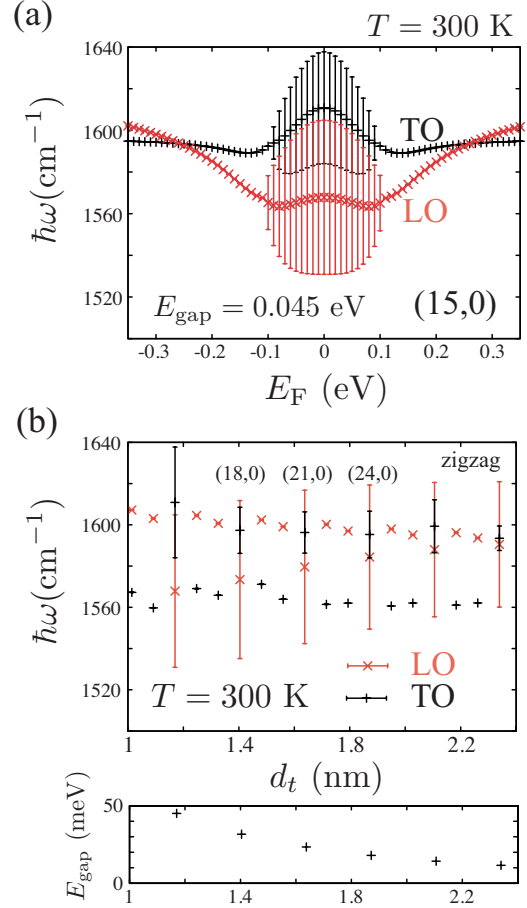


FIG. 4. (Color online) (a) The E_F dependence of the LO (red curve) and TO (black curve) phonon frequency for a (15,0) zigzag nanotube. Not only the frequency of the LO mode but also that of the TO mode is shifted due to the curvature effect. (b) The diameter d_t dependence of the phonon frequency for zigzag nanotubes, including zigzag semiconducting tubes. E_{gap} denotes the curvature-induced minienergy gap.

LO mode couples to an electron-hole pair and the TO mode is not coupled to an electron-hole pair for armchair SWNTs.

In Fig. 4(a), we show calculated results for $\hbar\omega_\lambda$ as a function of E_F for a (15,0) metallic zigzag nanotube. In the case of zigzag nanotubes, not only the LO mode but also the TO mode couples with electron-hole pairs. The spectrum peak position for the TO mode becomes harder for $E_F = 0$, since $\text{Re}[h(E)]$ for $E < \hbar\omega_{\text{TO}}$ contributes to a positive frequency shift. It has been shown theoretically²⁴ and experimentally²⁵ that even for “metallic” zigzag nanotubes a finite curvature opens a small energy gap. When the curvature effect is taken into account, the cutting line does not lie on the K point but is shifted from the k_2 axis. In this case, $\cos \theta(\mathbf{k}) = k_1 / (k_1^2 + k_2^2)^{1/2}$ is nonzero for the lower energy intermediate electron-hole pair states due to $k_1 \neq 0$. Thus, the TO mode can couple to the low energy electron-hole pair which makes a positive-energy contribution to the phonon energy shift. The high-energy electron-hole pair is still decoupled from the TO mode since $\cos \theta(\mathbf{k}) \rightarrow 0$ for $|k_2| \gg |k_1|$. Therefore, when $|E_F| \lesssim \hbar\omega_{\text{TO}}/2$, then $\hbar\omega_{\text{TO}}$ increases by a larger amount than $\hbar\omega_{\text{LO}}$. The TO mode for small diameter zigzag nanotubes

couples strongly with an electron-hole pair because of the stronger curvature effect. In Fig. 4(b), we show the diameter (d_t) dependence of the $\hbar\omega_\lambda$ of zigzag nanotubes for $E_F=0$ not only for metallic SWNTs, but also for semiconducting SWNTs. In the case of the semiconducting nanotubes, the LO (TO) mode appears at around 1600 (1560) cm^{-1} without any broadening. Only the metallic zigzag nanotubes show an energy shift, and the energy of the LO (TO) mode decreases (increases) as compared to the semiconducting tubes. In the lower part of Fig. 4(b), we show the curvature-induced energy gap E_{gap} as a function of d_t . The results show that higher (lower) energy electron-hole pairs contribute effectively to the LO (TO) mode softening (hardening) in metallic nanotubes. In the case of semiconducting nanotubes, we may expect that there is a softening for the LO and TO modes according to Eq. (2). However, the softening is small as compared with that of the metallic nanotubes because the energy of intermediate electron-hole pair states is much larger than $\hbar\omega_\lambda^{(0)}$ in this case.

III. CHIRALITY DEPENDENCE OF THE ELECTRON-PHONON INTERACTION

Here, we derive Eq. (2) on the basis of an effective-mass theory for π electrons near the K point in graphene. In a continuous model, the local modulation of the hopping integral due to lattice vibrations appears as a deformation-induced gauge field, $\mathbf{A}(\mathbf{r})=[A_x(\mathbf{r}), A_y(\mathbf{r})]$, in the Weyl equation.²⁶ The Weyl equation for π -electrons with energy eigenvalue E is written by

$$v_F \boldsymbol{\sigma} \cdot [\hat{\mathbf{p}} + \mathbf{A}(\mathbf{r})] \Psi(\mathbf{r}) = E \Psi(\mathbf{r}), \quad (3)$$

where v_F ($\equiv \gamma_0 \ell / \hbar$) is the Fermi velocity and γ_0 (≈ 2.7 eV) is the nearest-neighbor hopping integral, $\ell \equiv (3/2)a_{\text{cc}}$, $\hat{\mathbf{p}} = -i\hbar\nabla$ is the momentum operator, and $\boldsymbol{\sigma} = (\sigma_x, \sigma_y)$ is the Pauli matrix. $\mathbf{A}(\mathbf{r})$ is given in Eq. (3) of Ref. 27 by a small change $\delta\gamma_0^a(\mathbf{r})$ ($a=1,2,3$) in the hopping integral from $-\gamma_0$ (see Fig. 5) as

$$v_F A_x(\mathbf{r}) = \delta\gamma_0^1(\mathbf{r}) - \frac{1}{2}[\delta\gamma_0^2(\mathbf{r}) + \delta\gamma_0^3(\mathbf{r})],$$

$$v_F A_y(\mathbf{r}) = \frac{\sqrt{3}}{2}[\delta\gamma_0^2(\mathbf{r}) - \delta\gamma_0^3(\mathbf{r})]. \quad (4)$$

Here $\delta\gamma_0^a(\mathbf{r})$ for the LO and TO modes is given by $\delta\gamma_0^a(\mathbf{r}) = (g/\ell)\mathbf{u}(\mathbf{r}) \cdot \mathbf{R}_a$, where \mathbf{R}_a denotes the nearest-neighbor vectors (Fig. 5) and $\mathbf{u}(\mathbf{r})$ is the relative displacement vector of a B site from an A site [$\mathbf{u}(\mathbf{r}) = \mathbf{u}_B(\mathbf{r}) - \mathbf{u}_A(\mathbf{r})$] and g is the el-ph coupling constant. We rewrite Eq. (4) as

$$v_F [A_x(\mathbf{r}), A_y(\mathbf{r})] = g [u_y(\mathbf{r}), -u_x(\mathbf{r})], \quad (5)$$

where $u_i(\mathbf{r}) \equiv \mathbf{u}(\mathbf{r}) \cdot \mathbf{e}_i$, ($i=x, y$), and $\mathbf{R}_1 - (\mathbf{R}_2 + \mathbf{R}_3)/2 = \ell \mathbf{e}_y$ and $\sqrt{3}/2(\mathbf{R}_2 - \mathbf{R}_3) = \ell \mathbf{e}_x$ have been used (see Fig. 5). Then, the el-ph interaction for an in-plane lattice distortion $\mathbf{u}(\mathbf{r})$ can be rewritten as the vector product of $\boldsymbol{\sigma}$ and $\mathbf{u}(\mathbf{r})$,¹⁰

$$\mathcal{H}_{\text{int}} = v_F \boldsymbol{\sigma} \cdot \mathbf{A}(\mathbf{r}) = g [\boldsymbol{\sigma} \times \mathbf{u}(\mathbf{r})] \cdot \mathbf{e}_z. \quad (6)$$

We consider the LO and TO phonon modes with $\mathbf{q}=0$ (i.e., Γ point). Then, an electron-hole pair is excited by a

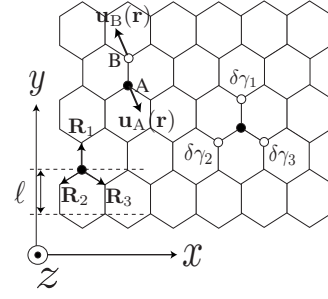


FIG. 5. A hexagonal unit cell of graphene consists of A (closed circle) and B (open circle) sublattices. \mathbf{R}_a ($a=1,2,3$) are vectors pointing to the nearest-neighbor B sites from an A site [$\mathbf{R}_1 = a_{\text{cc}}\mathbf{e}_y$, $\mathbf{R}_2 = -(\sqrt{3}/2)a_{\text{cc}}\mathbf{e}_x - (1/2)a_{\text{cc}}\mathbf{e}_y$, and $\mathbf{R}_3 = (\sqrt{3}/2)a_{\text{cc}}\mathbf{e}_x - (1/2)a_{\text{cc}}\mathbf{e}_y$]. Local modulations of the hopping integral are defined by $\delta\gamma_0^a(\mathbf{r})$ ($a=1,2,3$). The modulation is given by optical phonon modes as $\delta\gamma_0^a = (g/\ell)\mathbf{u}(\mathbf{r}) \cdot \mathbf{R}_a$, where $\mathbf{u}(\mathbf{r}) = [\mathbf{u}_A(\mathbf{r}) - \mathbf{u}_B(\mathbf{r})]$ is a relative displacement vector of a B site relative to the nearest A site.

constant $\mathbf{u} = (u_x, u_y)$, which corresponds to the A_{1g} phonon modes. The el-ph matrix element for the electron-hole pair generation is given by

$$\langle \text{eh}(\mathbf{k}) | \mathcal{H}_{\text{int}} | \omega \rangle = \int \Psi_{c,\mathbf{k}}^*(\mathbf{r}) \mathcal{H}_{\text{int}} \Psi_{v,\mathbf{k}}(\mathbf{r}) d^2\mathbf{r}$$

$$= \frac{g}{2} (e^{+i\Theta(\mathbf{k})/2} \quad e^{-i\Theta(\mathbf{k})/2}) \begin{pmatrix} 0 & u_y + iu_x \\ u_y - iu_x & 0 \end{pmatrix}$$

$$\times \begin{pmatrix} e^{-i\Theta(\mathbf{k})/2} \\ -e^{+i\Theta(\mathbf{k})/2} \end{pmatrix}, \quad (7)$$

where $\Psi_{c,\mathbf{k}}(\mathbf{r})$ [$\Psi_{v,\mathbf{k}}(\mathbf{r})$] denotes an energy eigenstate of $v_F \boldsymbol{\sigma} \cdot \mathbf{p}$ in the conduction (valence) energy band with energy eigenvalue $E = v_F |\mathbf{p}|$ ($E = -v_F |\mathbf{p}|$),

$$\Psi_{c,\mathbf{k}}(\mathbf{r}) = \frac{e^{i\mathbf{k} \cdot \mathbf{r}}}{\sqrt{2S}} \begin{pmatrix} e^{-i\Theta(\mathbf{k})/2} \\ e^{+i\Theta(\mathbf{k})/2} \end{pmatrix},$$

$$\Psi_{v,\mathbf{k}}(\mathbf{r}) = \frac{e^{i\mathbf{k} \cdot \mathbf{r}}}{\sqrt{2S}} \begin{pmatrix} e^{-i\Theta(\mathbf{k})/2} \\ -e^{+i\Theta(\mathbf{k})/2} \end{pmatrix}, \quad (8)$$

where S denotes the total area of the system, and $k_x - ik_y \equiv |\mathbf{k}| e^{-i\Theta(\mathbf{k})}$.

We first consider the case of a zigzag nanotube in Fig. 5. Then, we denote x (y) as a coordinate around (along) the axis [so that $\Theta(\mathbf{k}) = \theta(\mathbf{k})$], and $u_x(\mathbf{r})$ [$u_y(\mathbf{r})$] are assigned to the TO (LO) phonon mode. The corresponding $\mathbf{A}(\mathbf{r})$ for $u_x(\mathbf{r})$ and $u_y(\mathbf{r})$ are $A_y(\mathbf{r})$ and $A_x(\mathbf{r})$, respectively. By calculating Eq. (7) for the TO mode with $(u_x, u_y) = (u, 0)$ and for the LO mode with $(u_x, u_y) = (0, u)$, we get Eq. (2). Next, we consider the case of an armchair nanotube. Then, x (y) is the coordinate along (around) the axis [so that $\Theta(\mathbf{k}) = \theta(\mathbf{k}) + \pi/2$], and $u_x(\mathbf{r})$ [$u_y(\mathbf{r})$] is assigned to the LO (TO) phonon mode. The direction of the gauge field $\mathbf{A}(\mathbf{r})$ is perpendicular to the phonon eigenvector $\mathbf{u}(\mathbf{r})$ and the LO mode shifts the wave vector around the tube axis, which explains how the LO mode may induce a dynamical energy-band gap in metallic nanotubes.^{15,28} By calculating Eq. (7) for the TO mode with $(u_x, u_y) = (0, u)$ and for the LO mode with $(u_x, u_y) = (u, 0)$, we

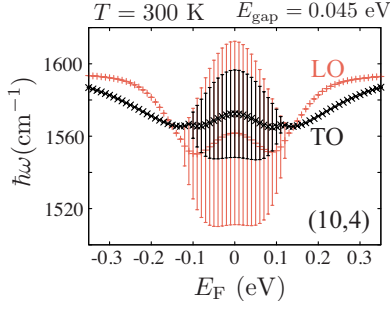


FIG. 6. (Color online) The E_F dependence of the LO (red curve) and TO (black curve) phonon energy for the (10,4) metallic chiral nanotube. E_{gap} denotes the curvature-induced minienergy gap which has the same value as that for the (15,0) tube in Fig. 4(a). The difference between the behavior of the (10,4) and (15,0) nanotubes comes from the fact that the phonon eigenvector of the LO (TO) mode is not pointing along the tube axis in the case of the (10,4) tube.

get Eq. (2), too. Equation (2) is valid regardless of the tube chirality if the phonon eigenvector of the LO (TO) phonon mode is in the direction along (around) the tube axis. This is because $\hat{\mathbf{p}}$ and $\mathbf{u}(\mathbf{r})$ are transformed in the same way as we change the chiral angle. As a result, there would be no chiral angle dependence for the el-ph coupling on Eq. (2).

However, the phonon eigenvector depends on the chiral angle. Reich *et al.*²⁰ reported that, for a chiral nanotube, atoms vibrate along the direction of the carbon-carbon bonds and not along the axis or the circumference. In the case of a chiral nanotube, the phonon eigenvector may be written as

$$\begin{pmatrix} u_{\text{TO}} \\ u_{\text{LO}} \end{pmatrix} = \begin{pmatrix} \cos \phi & \sin \phi \\ -\sin \phi & \cos \phi \end{pmatrix} \begin{pmatrix} u_1 \\ u_2 \end{pmatrix}, \quad (9)$$

where u_1 (u_2) is in the direction around (along) a chiral tube axis, and ϕ is the angle difference between the nanotube axis and the vibration. This modifies Eq. (2) as

$$\langle e(\mathbf{k}) | \mathcal{H}_{\text{int}} | \omega_{\text{LO}} \rangle = -igu \sin(\theta(\mathbf{k}) + \phi),$$

$$\langle e(\mathbf{k}) | \mathcal{H}_{\text{int}} | \omega_{\text{TO}} \rangle = -igu \cos(\theta(\mathbf{k}) + \phi). \quad (10)$$

In Fig. 6, we show numerical results for $\hbar\omega_\lambda$ as a function of E_F for a (10,4) metallic chiral nanotube for $T=300$ K. The energy difference between the minimum point at $E_F = \hbar\omega^{(0)}/2$ and at $E_F=0$ shows that the LO mode couples more strongly to the low energy electron-hole pair than the TO mode. Since the curvature-induced minienergy gap for (10,4) and (15,0) tubes are almost the same ($E_{\text{gap}}=0.045$ eV), we may expect a similar energy shift of the LO and TO modes. However, the results of the (15,0) zigzag tube show that the TO mode couples more strongly for the low-energy electron-hole pair than the LO mode. This is explained not by Eq. (2) but by Eq. (10) with an appropriate ϕ ($\phi \approx 23.4^\circ$), which is given by the phonon eigenvector calculation. Since the chiral angle for (10,4) is 16.1° , ϕ is not directly related to the chiral angle. The identification of ϕ in Eq. (10) as a function of nanotube chirality would be useful to compare theoretical results and experiments, which will be explored in the future.

IV. DISCUSSION

The phonon frequencies with some broadening as shown in Fig. 2 are not directly related to the Raman spectra of the G band but are related to the phonon density of states of the LO and TO phonons at $\mathbf{q}=0$. In previous papers,²⁹ we have shown that the G -band intensity depends on chiral angle for which for zigzag nanotubes the LO (TO) phonon mode intensity is strong (suppressed), while for armchair nanotubes the TO (LO) phonon mode intensity is strong (comparable). This chirality dependence of the G -band intensity is also observed in single nanotube Raman spectroscopy.^{30,31} This chirality dependence of the G -band mode intensity is exactly opposite to the chirality dependence of the phonon-softening for which the TO phonon mode is suppressed in armchair nanotubes. These observations clearly show that the corresponding el-ph interaction for phonon-softening and Raman processes are independent of each other. In the following, we will show that not only the LO mode but also the TO mode becomes Raman-active for armchair nanotubes due to the trigonal warping effect.

In the Raman process, the phonon is emitted by scattering an electron (or an exciton) from one conduction-band state to another conduction-band state, while in the phonon softening, the electron is scattered (or excited) from a valence-band state to a conduction-band state. Thus the corresponding matrix element for the Raman process is expressed by substituting $\Psi_{c,\mathbf{k}}(\mathbf{r})$ in Eq. (11) for $\Psi_{v,\mathbf{k}}(\mathbf{r})$ in Eq. (7) as follows:

$$\begin{aligned} \langle e(\mathbf{k}), \omega | \mathcal{H}_{\text{int}} | e(\mathbf{k}) \rangle &= \int \Psi_{c,\mathbf{k}}^*(\mathbf{r}) \mathcal{H}_{\text{int}} \Psi_{c,\mathbf{k}}(\mathbf{r}) d^2\mathbf{r} \\ &= \frac{g}{2} \begin{pmatrix} e^{+i\theta(\mathbf{k})/2} & e^{-i\theta(\mathbf{k})/2} \end{pmatrix} \\ &\quad \times \begin{pmatrix} 0 & u_y + iu_x \\ u_y - iu_x & 0 \end{pmatrix} \begin{pmatrix} e^{-i\theta(\mathbf{k})/2} \\ e^{+i\theta(\mathbf{k})/2} \end{pmatrix}. \end{aligned} \quad (11)$$

Then the electron-phonon matrix element for the Raman-scattering process becomes

$$\langle e(\mathbf{k}), \omega_{\text{LO}} | \mathcal{H}_{\text{int}} | e(\mathbf{k}) \rangle = gu \cos \theta(\mathbf{k}),$$

$$\langle e(\mathbf{k}), \omega_{\text{TO}} | \mathcal{H}_{\text{int}} | e(\mathbf{k}) \rangle = -gu \sin \theta(\mathbf{k}). \quad (12)$$

It is stressed again that the el-ph interactions of Eqs. (2) and (12) are for phonon-softening and Raman intensity, respectively, and that they are independent of each other. When we consider the Raman-scattering processes for carbon nanotubes, the \mathbf{k} vector which is relevant to the resonance Raman process is the \mathbf{k} vector at the van Hove singular point, \mathbf{k}_{ii} , which corresponds to the touching points of the equienergy surface to the cutting line (one-dimensional Brillouin zone plotted in the 2D BZ),^{1,32} which are shown in Figs. 7(a) and 7(b) for zigzag and armchair nanotubes, respectively.

In the case of the zigzag nanotubes, the \mathbf{k}_{ii} point corresponds to $\theta=0$ which is not the chiral angle but is defined in Fig. 3(b). Thus from Eq. (12), we see that the TO mode is not excited. On the other hand, in the case of the armchair nanotube, the value of θ is not zero because of the trigonally

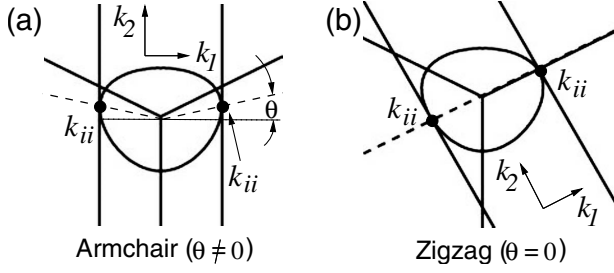


FIG. 7. Trigononal warping effect of an equienergy surface in the 2D Brillouin zone and cutting lines for (a) armchair and (b) zigzag nanotubes. In the case of (a) armchair nanotubes, the θ value defined from the k_1 axis in Fig. 5 is not zero while in the case of (b) zigzag nanotubes, θ is always zero, which explains the chirality dependence of the relative Raman intensity of LO and TO phonon modes.

warped equienergy surface, as shown in Fig. 7(b).^{1,32} Thus not only the LO but also the TO phonon modes can be observed, which is consistent with the previous experimental results^{30,31} and the theories.^{1,32} Thus when we see the G -band Raman spectra for metallic nanotubes, we can expect the following features: for armchair nanotubes, we can see both the LO and TO modes in which the LO mode appears at a lower frequency region with some spectral width, while the TO mode appears without spectral broadening because of the absence of phonon softening. For zigzag nanotubes, we can see only a broadened LO phonon mode but we cannot see a TO phonon mode. For a general chiral nanotube, we generally observe both the LO and TO phonon modes with some broadening as a function of θ . Further, we expect some phonon hardening effect for the TO phonon mode. The relative intensity between the LO and TO phonon modes is determined by the chirality dependent Raman intensity and spectral width. The detailed Raman spectral features for all metallic (n,m) nanotubes will be presented elsewhere.

The gauge-field descriptions for the lattice deformation [Eq. (4)] and for the el-ph interaction of the LO and TO modes [Eq. (5)] are useful to show the appearance of the curvature-induced minienergy gap in metallic zigzag carbon nanotubes and the decoupling between the TO mode with a finite wave vector and the electrons, as shown in the following. For a zigzag nanotube, we have $\delta\gamma_0^1=0$ and $\delta\gamma_0^2=\delta\gamma_0^3$ from the rotational symmetry around the tube axis (see Fig. 5). Then, Eq. (4) shows that for $A_x \neq 0$ and $A_y=0$, the cutting line of $k_x=0$ for the metallic zigzag nanotube is shifted by a finite constant value of A_x because of the Aharonov-Bohm effect for the lattice distortion-induced gauge field \mathbf{A} . This explains the appearance of the curvature-induced minienergy gap in metallic zigzag carbon nanotubes³³ and of the phonon broadening for the TO mode as a function of E_F . The TO phonon mode with $\mathbf{q} \neq 0$ does not change the area of the hexagonal lattice but instead gives rise to a shear deformation. Thus, the TO mode [$\mathbf{u}_{\text{TO}}(\mathbf{r})$] satisfies

$$\nabla \cdot \mathbf{u}_{\text{TO}}(\mathbf{r}) = 0, \quad \nabla \times \mathbf{u}_{\text{TO}}(\mathbf{r}) \neq 0. \quad (13)$$

Using Eqs. (5) and (13), we see that the TO mode does not yield the deformation-induced magnetic field [$\mathbf{B}(\mathbf{r}) = \nabla$

$\times \mathbf{A}(\mathbf{r})$] but the TO mode does yield a divergence of $\mathbf{A}(\mathbf{r})$ instead because

$$B_z(\mathbf{r}) = -\frac{g}{v_F} \nabla \cdot \mathbf{u}_{\text{TO}}(\mathbf{r}) = 0, \quad (14)$$

$$\nabla \cdot \mathbf{A}(\mathbf{r}) = \frac{g}{v_F} (\nabla \times \mathbf{u}_{\text{TO}}(\mathbf{r})) \cdot \mathbf{e}_z \neq 0.$$

Thus, we can set $\mathbf{A}(\mathbf{r}) = \nabla \varphi(\mathbf{r})$ where $\varphi(\mathbf{r})$ is a scalar function. Since we can set $\mathbf{A}(\mathbf{r}) = 0$ in Eq. (3) by a redefinition of the phase of the wave function (a local gauge symmetry) as $\Psi(\mathbf{r}) \rightarrow \exp[-i\varphi(\mathbf{r})/\hbar] \Psi(\mathbf{r})$,²⁶ and thus $\mathbf{A}(\mathbf{r})$ in Eq. (3) disappears for the TO mode with $\mathbf{q} \neq 0$. This explains why the TO mode with $\mathbf{q} \neq 0$ is completely decoupled from the electrons and that only the TO mode with $\mathbf{q} = 0$ couples with electrons. This conclusion is valid even when the graphene sheet has a static surface deformation. In this sense, the TO phonon mode at the Γ point is anomalous since the el-ph interaction for the TO mode cannot be eliminated by the phase of the wave function. It may be difficult to include the local gauge symmetry in a numerical analysis. On the other hand, the LO phonon mode with $\mathbf{q} \neq 0$ changes the area of the hexagonal lattice, while it does not give rise to a shear deformation. Thus, the LO mode ($\mathbf{u}_{\text{LO}}(\mathbf{r})$) satisfies

$$\nabla \cdot \mathbf{u}_{\text{LO}}(\mathbf{r}) \neq 0, \quad \nabla \times \mathbf{u}_{\text{LO}}(\mathbf{r}) = 0. \quad (15)$$

Using Eqs. (5) and (15), we see that the LO mode gives rise to a deformation-induced magnetic field since

$$B_z(\mathbf{r}) \neq 0, \quad \nabla \cdot \mathbf{A}(\mathbf{r}) = 0. \quad (16)$$

Since a magnetic field changes the energy-band structure of electrons, the LO mode (with $\mathbf{q} \neq 0$) couples strongly to the electrons.

In the case of 2D graphene, Eq. (2) tells us that the Γ point TO and LO modes give the same energy shift because the integral over $\theta(\mathbf{k})$ gives the same $\hbar\omega_\lambda^{(2)}$ in Eq. (1) for both TO and LO modes. This explains why no G -band splitting is observed in a single layer of graphene.³⁴ Even when we consider the TO and LO modes near the Γ point, we do not expect any splitting between the LO and TO phonon energies because the TO mode with $\mathbf{q} \neq 0$ is completely decoupled from the electrons. Thus, for $\mathbf{q} \neq 0$, only the LO mode contributes to the G band.

In our numerical results for $\hbar\omega_\lambda$, we see a crossing between the LO and TO modes at some values of E_F . If there is a finite transition amplitude between the LO and TO phonon modes, we need to diagonalize the following matrix according to second-order perturbation theory for a degenerate case,

$$\begin{pmatrix} \langle \omega_{\text{LO}} | \mathcal{H}^{(2)} | \omega_{\text{LO}} \rangle & \langle \omega_{\text{LO}} | \mathcal{H}^{(2)} | \omega_{\text{TO}} \rangle \\ \langle \omega_{\text{TO}} | \mathcal{H}^{(2)} | \omega_{\text{LO}} \rangle & \langle \omega_{\text{TO}} | \mathcal{H}^{(2)} | \omega_{\text{TO}} \rangle \end{pmatrix}, \quad (17)$$

where $\mathcal{H}^{(2)}$ is the effective Hamiltonian in second-order perturbation theory given by

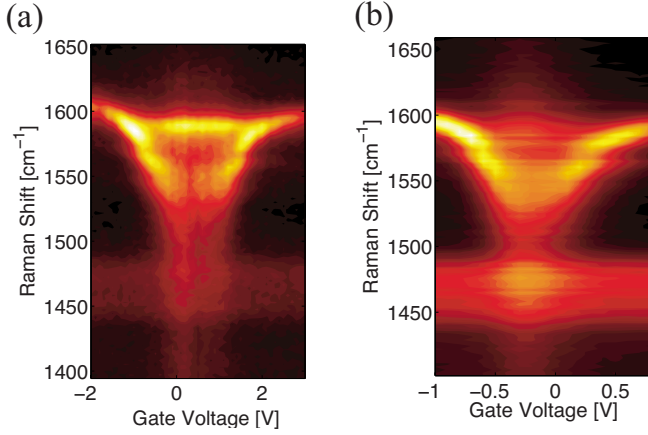


FIG. 8. (Color online) Experimental results for the Raman G -band intensity as a function of applied gate voltage for two metallic SWNTs (a) and (b). A strong (weak) intensity peak is denoted by the yellow (black) color.

$$\mathcal{H}^{(2)} = \sum_{\mathbf{k}} \frac{\mathcal{H}_{\text{int}}|\text{eh}(\mathbf{k})\rangle\langle\text{eh}(\mathbf{k})|\mathcal{H}_{\text{int}}}{\hbar\omega_{\lambda}^{(0)} - (E_e(\mathbf{k}) - E_h(\mathbf{k})) + i\Gamma}. \quad (18)$$

Using Eq. (2), we see that $\cos\theta(\mathbf{k})\sin\theta(\mathbf{k})$ which is an odd function of k_2 appears in the numerator for the off-diagonal terms in Eq. (17). Thus, the mode coupling through the electron-hole pair at k_2 is canceled by that at $-k_2$, i.e., due to the time-reversal symmetry of the system. Thus, even though the LO and TO modes cross each other, there is no mixing between the LO and TO phonon modes for any chirality. If there is a breaking of time-reversal symmetry for k_2 , we expect some mixing between the LO and TO phonon modes.

V. COMPARISON WITH EXPERIMENT AND SUMMARY

The first comparison we make is to experimental results in the literature. Here we try to assign the chirality of the nanotube that is given in Fig. 2 of Ref. 18. This figure shows two strong intensity peaks with different phonon frequencies. The higher-frequency peak does not depend on the gate voltage and the lower-frequency peak shows a frequency shift with a strong broadening near the Dirac point. The existence of a flat intensity peak as a function of Fermi energy for a metallic SWNT indicates that the electron-phonon coupling is very weak for the phonon mode. Thus, the nanotube can be thought of as an armchair SWNT (or close to an armchair SWNT with a chiral angle near 30°) since the el-ph coupling between the TO mode and electron-hole pairs is negligible in this case. Further investigation comparing theory with experiment is strongly necessary for tubes of different chiralities.

In Figs. 8(a) and 8(b), we show experimental results of the G -band intensity as a function of applied gate voltage for two different isolated SWNTs. For a given excitation energy

of 1.91 eV and the observed radial breathing mode (RBM) frequencies of 196 and 193 cm^{-1} for the sample of Figs. 8(a) and 8(b), respectively, we can assign (n,m) by using the conventional assignment technique that we used for single nanotube Raman spectroscopy.³⁵ As a result, we assign the (n,m) values as (12,6) for Fig. 8(a) and (15,3), (16,1), or (11,8) for Fig. 8(b).

Although (12,6) is not so close to the chiral angle for an armchair nanotube, we expect that Fig. 8(a) exhibits a similar behavior to that of Fig. 2 of Ref. 18. Thus the assignment of (12,6) from the RBM spectra is consistent with the present phonon spectra. In Fig. 8(b), the intensity near the Dirac point of the TO (LO) mode is weaker (stronger) than shown in Fig. 8(a). This indicates that the tube is not an armchair SWNT but close to a metallic zigzag SWNT (or a metallic chiral SWNT). Thus we can assign this SWNT either to (15,3) or to (16,1) for the SWNT for Fig. 8(b) and we can exclude (11,8). A further comparison with more experimental data will be required, which will be carried out in the future.

A chirality-dependent Raman intensity was observed for metallic SWNTs as shown in Fig. 1 of Ref. 36. Although the E_F positions for the observed metallic SWNTs are unclear, the results are consistent with our calculations in the following way. For example, the TO mode in a (15,15) SWNT gives a sharp line shape and the LO mode shows a broad feature for a (24,0) SWNT. It is noted that the Raman intensity is proportional to the el-ph coupling for an optically excited electron via Eq. (12). Since this el-ph coupling depends on the chiral angle due to the trigonal warping effect, one of the two optical modes may be invisible in the Raman intensity.^{36,37}

In summary, we have calculated the E_F dependence of $\hbar\omega_{\lambda}$ (λ =LO and TO) on metallic carbon nanotubes. The results show a strong dependence of the phonon frequency shift on the chirality of single-walled carbon nanotubes because of the curvature-induced shift of the wave vector around the tube axis. This is explained by the general property of second-order perturbation theory and the characteristic electron-phonon coupling for the Γ point LO and TO phonon modes [Eqs. (2) and (6)]. Since the frequency shift of the LO/TO phonon modes depends on the value of E_F , we think that the assignment of the LO/TO phonon modes to the G^-/G^+ bands should be defined for $E_F=0$ without any ambiguity. For the LO and TO phonon modes near the Γ point, we showed the absence of an electron-phonon coupling for the TO mode for $\mathbf{q}\neq 0$ due to a local gauge symmetry and that the LO mode works as a deformation-induced magnetic field. The phonon mixing between LO and TO phonon modes is absent in second-order perturbation theory due to time-reversal symmetry.

ACKNOWLEDGMENTS

R.S. acknowledges a Grant-in-Aid (Nos. 16076201 and 20241023) from MEXT. MIT authors acknowledge support from NSF under Grant No. DMR 07-04197.

- ¹R. Saito, G. Dresselhaus, and M. S. Dresselhaus, *Physical Properties of Carbon Nanotubes* (Imperial College Press, London, 1998).
- ²A. Jorio, M. A. Pimenta, A. G. Souza Filho, R. Saito, G. Dresselhaus, and M. S. Dresselhaus, *New J. Phys.* **5**, 139 (2003).
- ³R. Saito, A. Grüneis, Ge. G. Samsonidze, V. W. Brar, G. Dresselhaus, M. S. Dresselhaus, A. Jorio, L. G. Cançado, C. Fantini, M. A. Pimenta, and A. G. Souza Filho, *New J. Phys.* **5**, 157 (2003).
- ⁴A. Jorio, A. G. Souza Filho, G. Dresselhaus, M. S. Dresselhaus, A. K. Swan, M. S. Ünlü, B. Goldberg, M. A. Pimenta, J. H. Hafner, C. M. Lieber, and R. Saito, *Phys. Rev. B* **65**, 155412 (2002).
- ⁵R. Saito, C. Fantini, and J. Jiang, in *Carbon Nanotubes: Advanced Topics in the Synthesis, Structure, Properties and Applications*, Springer Series on Topics in Applied Physics Vol. 111, edited by Ado Jorio, M. S. Dresselhaus, and G. Dresselhaus (Springer-Verlag, Berlin, 2007), pp. 233–266.
- ⁶M. A. Pimenta, A. Marucci, S. A. Empedocles, M. G. Bawendi, E. B. Hanlon, A. M. Rao, P. C. Eklund, R. E. Smalley, G. Dresselhaus, and M. S. Dresselhaus, *Phys. Rev. B* **58**, R16016 (1998).
- ⁷S. D. M. Brown, A. Jorio, P. Corio, M. S. Dresselhaus, G. Dresselhaus, R. Saito, and K. Kneipp, *Phys. Rev. B* **63**, 155414 (2001).
- ⁸S. Piscanec, M. Lazzeri, F. Mauri, A. C. Ferrari, and J. Robertson, *Phys. Rev. Lett.* **93**, 185503 (2004).
- ⁹M. Lazzeri and F. Mauri, *Phys. Rev. Lett.* **97**, 266407 (2006).
- ¹⁰K. Ishikawa and T. Ando, *J. Phys. Soc. Jpn.* **75**, 084713 (2006).
- ¹¹V. N. Popov and P. Lambin, *Phys. Rev. B* **73**, 085407 (2006).
- ¹²N. Caudal, A. M. Saitta, M. Lazzeri, and F. Mauri, *Phys. Rev. B* **75**, 115423 (2007).
- ¹³A. Das, A. K. Sood, A. Govindaraj, A. M. Saitta, M. Lazzeri, F. Mauri, and C. N. R. Rao, *Phys. Rev. Lett.* **99**, 136803 (2007).
- ¹⁴P. C. Eklund, G. Dresselhaus, M. S. Dresselhaus, and J. E. Fischer, *Phys. Rev. B* **16**, 3330 (1977).
- ¹⁵O. Dubay, G. Kresse, and H. Kuzmany, *Phys. Rev. Lett.* **88**, 235506 (2002).
- ¹⁶O. Dubay and G. Kresse, *Phys. Rev. B* **67**, 035401 (2003).
- ¹⁷K. T. Nguyen, A. Gaur, and M. Shim, *Phys. Rev. Lett.* **98**, 145504 (2007).
- ¹⁸H. Farhat, H. Son, Ge. G. Samsonidze, S. Reich, M. S. Dresselhaus, and J. Kong, *Phys. Rev. Lett.* **99**, 145506 (2007).
- ¹⁹T. Ando, *J. Phys. Soc. Jpn.* **77**, 014707 (2008).
- ²⁰S. Reich, C. Thomsen, and P. Ordejón, *Phys. Rev. B* **64**, 195416 (2001).
- ²¹Ge. G. Samsonidze, R. Saito, N. Kobayashi, A. Grüneis, J. Jiang, A. Jorio, S. G. Chou, G. Dresselhaus, and M. S. Dresselhaus, *Appl. Phys. Lett.* **85**, 5703 (2004).
- ²²J. Jiang, R. Saito, Ge. G. Samsonidze, S. G. Chou, A. Jorio, G. Dresselhaus, and M. S. Dresselhaus, *Phys. Rev. B* **72**, 235408 (2005).
- ²³D. Porezag, Th. Frauenheim, Th. Köhler, G. Seifert, and R. Kaschner, *Phys. Rev. B* **51**, 12947 (1995).
- ²⁴R. Saito, M. Fujita, G. Dresselhaus, and M. S. Dresselhaus, *Phys. Rev. B* **46**, 1804 (1992).
- ²⁵M. Ouyang, J. L. Huan, C. L. Cheung, and C. M. Lieber, *Science* **292**, 702 (2001).
- ²⁶K. Sasaki, Y. Kawazoe, and R. Saito, *Prog. Theor. Phys.* **113**, 463 (2005).
- ²⁷K. Sasaki, S. Murakami, and R. Saito, *J. Phys. Soc. Jpn.* **75**, 074713 (2006).
- ²⁸S. Roche *et al.*, *J. Phys.: Condens. Matter* **19**, 182203 (2007).
- ²⁹R. Saito, A. Jorio, J. H. Hafner, C. M. Lieber, M. Hunter, T. McClure, G. Dresselhaus, and M. S. Dresselhaus, *Phys. Rev. B* **64**, 085312 (2001).
- ³⁰Z. Yu and L. E. Brus, *J. Phys. Chem. B* **105**, 1123 (2001).
- ³¹A. Jorio, M. A. Pimenta, C. Fantini, M. Souza, A. G. Souza Filho, Ge. G. Samsonidze, G. Dresselhaus, M. S. Dresselhaus, and R. Saito, *Carbon* **42**, 1067 (2004).
- ³²Ge. G. Samsonidze, R. Saito, A. Jorio, M. A. Pimenta, A. G. Souza Filho, A. Grüneis, G. Dresselhaus, and M. S. Dresselhaus, *J. Nanosci. Nanotechnol.* **3**, 431 (2003).
- ³³C. L. Kane and E. J. Mele, *Phys. Rev. Lett.* **78**, 1932 (1997).
- ³⁴J. Yan, Y. Zhang, P. Kim, and A. Pinczuk, *Phys. Rev. Lett.* **98**, 166802 (2007).
- ³⁵A. Jorio, R. Saito, J. H. Hafner, C. M. Lieber, M. Hunter, T. McClure, G. Dresselhaus, and M. S. Dresselhaus, *Phys. Rev. Lett.* **86**, 1118 (2001).
- ³⁶Y. Wu, J. Maultzsch, E. Knoesel, B. Chandra, M. Huang, M. Y. Sfeir, L. E. Brus, J. Hone, and T. F. Heinz, *Phys. Rev. Lett.* **99**, 027402 (2007).
- ³⁷S. Reich and C. Thomsen, *Philos. Trans. R. Soc. London, Ser. A* **362**, 2271 (2004).